Hindawi
Advances in Civil Engineering
Volume 2020, Article ID 6347597, 9 pages
https://doi.org/10.1155/2020/6347597

Research Article

Shrinkage Mechanism of Laterite Modified by Lime and Metakaolin

Yunzhi Tan,[1] **Yan Hu**,[1] **Rui Chen**,[1] **and Wenjing Sun**[2]

[1]*College of Civil Engineering and Architecture, China Three Gorges University, 8 University Road, Yichang 443002, China*
[2]*Department of Civil Engineering, Shanghai University, Shanghai 200433, China*

Correspondence should be addressed to Yunzhi Tan; yztan@ctgu.edu.cn

Received 22 February 2020; Accepted 24 June 2020; Published 24 July 2020

Academic Editor: Junhui Zhang

Copyright © 2020 Yunzhi Tan et al. This is an open access article distributed under the Creative Commons Attribution License, which permits unrestricted use, distribution, and reproduction in any medium, provided the original work is properly cited.

In this study, effects of metakaolin and lime on the microstructural characteristics, unconfined compressive strength (UCS), shrinkage, suction, and shear resistance of laterite were investigated. Soil samples treated with 5 wt% of lime (LaL) or 4 wt% metakaolin and 5 wt% of lime (LaLM) were prepared. Samples with an optimal water content of 32% were compacted and cured for 180 days, followed by saturation and dehydration until the desirable water content of the samples was attained. Then, the UCS, shrinkage, and suction and shear resistance of the samples at a normal stress of 200 kPa were determined. In addition, scanning electron microscopy imaging as well as mercury intrusion porosimetry tests were performed to examine the microstructural changes. Results indicate that the shrinkage of treated soil samples is significantly improved in comparison with that of the untreated soil samples. Lime effectively improves the UCS and shearing resistance of laterite. Moreover, metakaolin is composed of amorphous silicon and aluminium oxides and shared edge-face structures on the microscopic scale; hence, it can considerably capture calcium ions from a lime solution, generating cementitious hydrates in the interaggregates of laterite. Results also revealed that the combination of 5 wt% of lime and 4 wt% of metakaolin can improve the UCS and shearing resistance, but the linear shrinkage is particularly restrained, significantly decreasing by 4 times compared with that of the lime-treated soil sample and by 8 times compared with that of the untreated soil sample. The study results demonstrate that metakaolin and lime can be effectively used to improve laterite in lieu of the conventional lime treatment for mitigating geotechnical engineering disasters.

1. Introduction

Laterite is the weathered product on parent rocks in hot and wet tropical climates. It contains not only silicon and aluminium oxides but also cementitious materials such as free iron oxide; hence, it exhibits a red colour [1]. It is widely distributed in China (Hunan, Yunnan, and Guizhou provinces, as well as Guangxi Autonomous Region) and spans an area of 1.08 million square kilometres [2]. Laterite is present in problematic soil, and it exhibits high water sensitivity: It becomes mired when it absorbs a large amount of water, and it shrinks and cracks when it loses water. Moreover, under the long-term alternation of atmospheric rainfall and evaporation as well as other environmental factors, laterite can lead to engineering accidents, such as decreased foundation bearing capacity, slope cracking, and collapse [3, 4]. Therefore, it is imperative to decrease or control the water sensitivity of laterite.

The water sensitivity of laterite is characterised by miring and water loss shrinkage [5]. It is widely accepted that the lower the water content, the greater the matrix suction, and the higher the strength of the unsaturated soil [6, 7]. Thus, several researchers only focus on miring and believe that the possibility of engineering accidents can be decreased as long as the migration or permeation of water in the soil is prevented. However, the shrinkage cracking behaviour of clay is extremely distinct [8, 9]. Some studies have reported that water loss shrinkage mainly causes a change in the pore structure of interaggregates rather than in that of intra-aggregates in compacted laterite [10]. Although the loss of water increases the matrix suction, it results in shrinkage and cracking, leading to irreversible structural damage in

compacted laterite. Thus, the increase in the matrix suction and crack occurrence exerts opposite effects on the strength of compacted laterite. That is, the cracking behaviour caused by the water loss shrinkage also should be considered. Recently, researchers have reported that the shrinkage of laterite can be hindered by the improvement of the initial compactness water content or even adding some material such as gravel [11–13]. In addition, the shrinkage of laterite can be effectively ameliorated by the addition of lime [14], but whether lime-modified laterite can be applied in practical engineering projects needs to be investigated further.

Metakaolin exhibits high pozzolanic activity. When kaolin is heated to 500°C–700°C, an amorphous material is produced. This material is 50–55% of SiO_2 and 40–45% of Al_2O_3 by weight, and it is extremely reactive in an alkaline calcium-rich solution. In [15–17], it is reported that metakaolin can efficiently absorb calcium hydroxide to consistently form a cementitious hydrate, and kaolin absorbs hydrated calcium ions, which form a layer on the clay particle surfaces and subsequently prevent the further dissolution of clay mineral platelets. Metakaolin-containing concretes exhibit behaviour similar to those of silica-fume-containing concretes; that is, the mechanical resistance is improved, and the permeability and shrinkage of concrete are significantly reduced [18]. However, whether metakaolin effectively impacts water sensitivity is not known. Therefore, strength and shrinkage tests under different moisture conditions on compacted specimens are conducted in this study. Meanwhile, the variation in suction was measured, and microscopic tests were performed. Finally, the aforementioned formal tests revealed the shrinkage mechanism of lime and metakaolin modified laterite.

2. Materials and Methods

2.1. Materials. Laterite was obtained from Guilin, Guangxi Autonomous Region (China). By X-ray fluorescence, its chemical composition was determined to predominantly comprise silicon aluminium oxide (74 wt%) and iron oxide (19 wt%) (Table 1). After the dried laterite was passed through a 0.5 mm sieve, its fundamental properties were measured according to the Chinese standard JTG E40-2007. Table 2 summarizes the results. As the liquid limit of laterite exceeded 50% herein, it was defined as a high liquid limit soil. Furthermore, its optimum water content (30.2%) and maximum dry density (1.48 g/cm^3) were obtained by heavy compaction tests (Figure 1).

Lime was purchased from Suqian, Jiangsu Province (China), and its chemical composition was predominantly CaO (98.34 wt%), with a small amount of Al_2O_3 (0.57 wt%). Its specific gravity was 2.32, and its initial water content was 3.1%. Metakaolin was purchased from Royal Dutch Shell plc, and its chemical composition was predominantly Al_2O_3 (46.2 wt%) and SiO_2 (49.5 wt%). Its specific gravity was 2.63, and its initial water content was 1.5%. The particle distribution characteristics of laterite, lime, and metakaolin were investigated using a Microtrac S3500 particle size analyser (Figure 2).

Table 1: Major components of laterite.

Composition	Al_2O_3	SiO_2	Fe_2O_3	TiO_2	K_2O	Others
Mass content (%)	40.6	33.3	19.1	2.4	2.1	2.5

2.2. Sample Preparation. To investigate the effects of metakaolin and lime on the shrinkage of laterite, six kinds of specimens were prepared (Table 3). Due to the different specific gravities of laterite, lime, and metakaolin, the specific gravity of mixed soil (G_m) was calculated as follows:

$$G_m = \frac{1}{\left((1 - R_l - R_{mk})/G_{la}\right) + \left(R_l/G_l\right) + \left(R_{mk}/G_{mk}\right)}, \quad (1)$$

where G_{mk}, G_l, and G_{la} are the specific gravities of metakaolin, lime, and laterite, respectively, and R_{mk} and R_l are the mixing ratios (wt%) of metakaolin and lime, respectively.

The relationship between the dry density (ρ_d) and initial void ratio (e_0) was calculated as follows:

$$\rho_d = \frac{G_m}{1 + e_0}. \quad (2)$$

For comparison of test results, all compacted samples have the same initial void ratio. To be more specific, the initial dry density of the laterite specimens was 1.43 g/cm^3, while those of the laterite-lime specimens and laterite-lime-metakaolin specimens were 1.422 g/cm^3 and 1.420 g/cm^3, respectively.

In this study, the soil samples were dry mixed, and then water was added to the mixture soils until the predicted water content was attained to achieve sample moisture conditions. Finally, the mixtures of metakaolin and/or lime-laterite with deionized water were compacted layer by layer in a sample compaction container until soil samples were obtained with dimensions of 61.8 mm (diameter) × 20 mm (height) and 50 mm (diameter) × 50 mm (height) with an initial water content of 32%. Pure laterite samples were prepared in the same manner as the control samples. All test samples exhibited the same initial void ratio to ensure that different samples exhibited the same initial pore volume.

2.3. Experimental Procedures. In this experiment, after compaction, all specimens were sealed and cured for 180 days at 25°C, which was followed by a saturation process. Then, each test was conducted as follows:

(1) Shrinkage tests were conducted according to the Chinese standard JTG E40-2007 [19].

(2) For the UCS tests and suction measurements, some specimens were placed in a chamber at a constant temperature (55°C), and then their mass was estimated to determine the real-time water content during dehydration. When the real-time water content approached the predetermined value, the samples were sealed and cured for 2 months in the chamber at 25°C to ensure homogeneity. Then, 10–20 g of each sample was used for suction measurement using a Decagon WP4C dewpoint potentiometer.

Table 2: Basic properties of laterite.

Proportion	Liquid limit (%)	Plastic limit (%)	Free swell (%)	Optimum moisture content (%)	Maximum dry density
2.71	56.5	35.4	16.9	30.2	1.48 g/cm^3

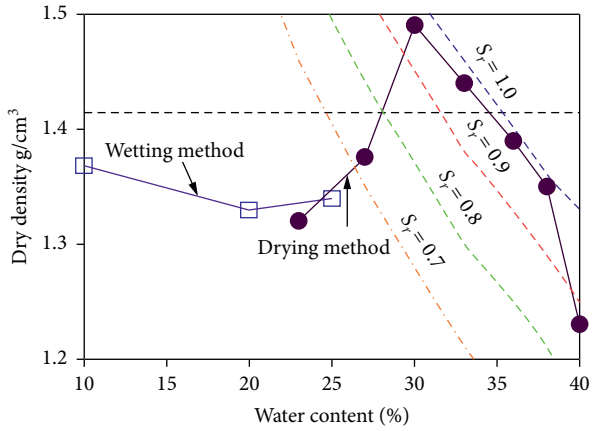

Figure 1: Compaction curves of laterite.

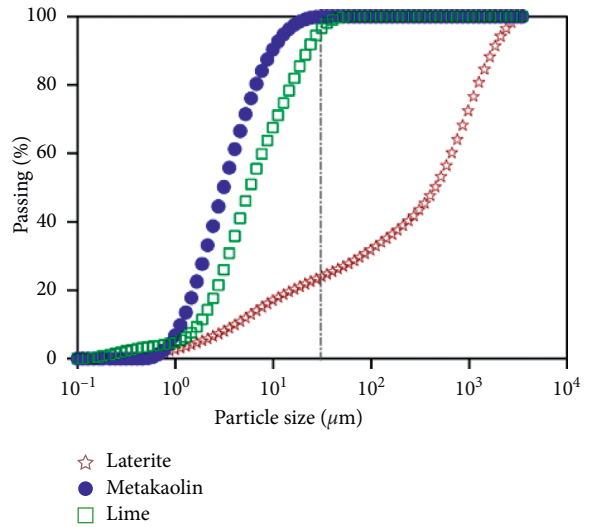

Figure 2: Particle size distribution curves of testing materials.

(3) For direct shear tests, some samples were dehydrated by the vapor equilibrium method (Table 4). When the soil suction became constant (determined by the stabilization of the specimen mass), direct shear tests were conducted at a shear rate of 0.8 mm/min under a vertical stress of 200 kPa.

(4) For pore analysis tests, after the specimens were freeze-dried for 1 day, a small block was used to obtain the pore size distribution with a Pore Master (PM 60GT) system.

(5) For scanning electron microscopy (SEM) imaging, to directly determine the reaction mechanism in the treated soil, mixtures of compacted lime-kaolin and lime-metakaolin were used. Each sample was carefully cut into a size of 15 mm × 15 mm × 15 mm to avoid disturbance and ensure porosity. Then, the cut sample was placed into liquid nitrogen, and the sample was dried by using a vacuum freeze-drying device. After drying, the sample was used for SEM analysis.

To further investigate the mechanism of metakaolin and lime modification of laterite, X-ray diffraction (XRD) patterns, thermogravimetric analysis (TGA) curves, and infrared (IR) spectra were recorded to explain the manner in which metakaolin aids lime in restraining the shrinkage of laterite.

3. Results and Discussion

3.1. X-Ray Diffraction (XRD) Results. After the formation of metakaolin from kaolin by calcination at 500°C–700°C, XRD patterns were recorded, and the diffraction spectrum of metakaolin lacked clear diffraction peaks similar to those of kaolin (Figure 3). Before calcination, kaolin exhibited clear diffraction peaks characteristic of kaolin, but after calcination, these diffraction peaks disappeared, indicating that kaolin is transformed or disappeared during calcination. Konan et al. [17] has reported the comparison of surface properties between kaolin and metakaolin in concentrated lime solutions and also reported a similar result. Kakali et al. [20] has confirmed that kaolin is transformed to metakaolin during calcination and becomes a high pozzolanic material.

3.2. Thermogravimetric Analysis (TGA) Results. To understand the characteristics of metakaolin, it is crucial to determine its composition and structure. Kaolin comprises feldspar and mica particles with alumina-rich elements or acidic igneous rocks. First, it undergoes weathering and disintegration, and it is then deposited from $Al(OH)_3$ and $Si(OH)_4$ in solution. Its chemical formula is $Si_2Al_2O_5(OH)_4$, and its molecular structure is shown in Figure 4.

Kaolin is transformed to metakaolin at high temperatures by dehumidification, which is expressed as follows:

$$Si_2Al_2O_5(OH)_4 \xrightarrow{500-700^\circ C} Si_2Al_2O_7 + 2H_2O \quad (3)$$

Thus, four hydroxyl groups are transformed into two water molecules and two oxygen anions remain in the material, as shown in the following chemical reaction:

$$4(OH^-) \longrightarrow 2H_2O + O^{2-} \quad (4)$$

In summary, the hydrogen bond connected to the basic structural unit disappears during dehumidification, and the laminated surface structure of kaolin is destroyed. Figure 5 shows the TGA curves of metakaolin and kaolin. The experimental test conditions were as follows: a TA thermogravimetric analyser (SDT Q600) was utilized at a heating rate of 10°C/min and a temperature range of 25°C–1000°C under nitrogen.

Table 3: Testing plan.

No.	Test name	Sample category	Initial state of sample
1	Shrinkage test	La LaL LaLM	$e_0 = 0.89$ $\omega = 32\%$ Ring knife sample (φ 61.8 mm × 20 mm)
2	Unconfined compression strength and suction test	Same as above	$e_0 = 0.89$ $\omega = 32\%$ Cylinder sample (φ 50 mm × 50 mm)
3	Direct shear test	Same as above	$e_0 = 0.89$ $\omega = 32\%$ Ring knife sample (φ 61.8 mm × 20 mm)
4	Pore analysis test	LaL LaLM	$e_0 = 0.89$ $\omega_1 = 0\%$, 28% Side length of the cube≈1.5 cm

Notice: e_0 is the porosity ratio after the sample was pressed, ω is the original water content after the sample was pressed, and ω_1 is the water content of the sample during dehydration.

Table 4: Saturated salt solution and corresponding suction values ($T = 25^{\circ}C$).

Solution	K_2SO_4	KCL	NaCl	KI	NaBr	K_2CO_3	$MgCl_2$	CH_3COOK	LiCl
Suction (MPa)	3.76	23.59	38.92	51.11	75.68	115.15	152.94	204.65	299.14

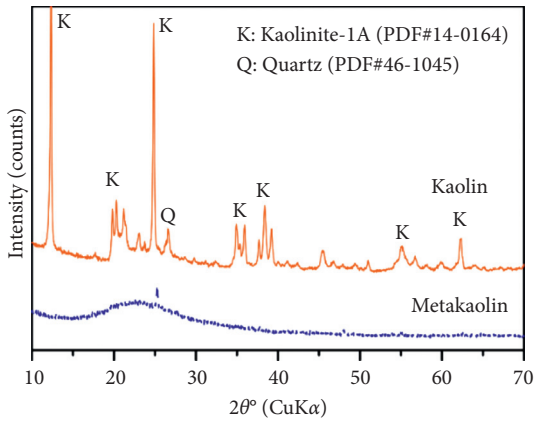

Figure 3: XRD pattern of kaolin and metakaolin.

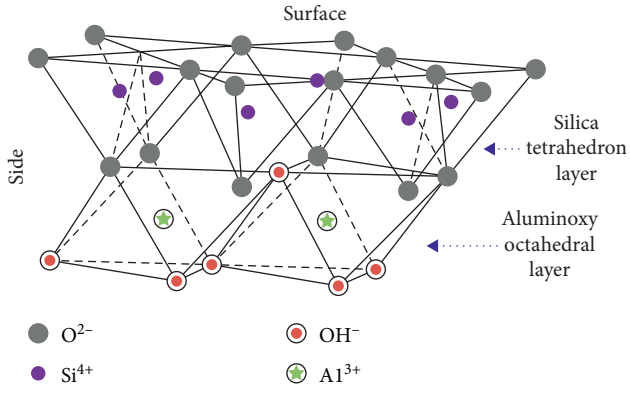

Figure 4: Basic structure unit of kaolin [21].

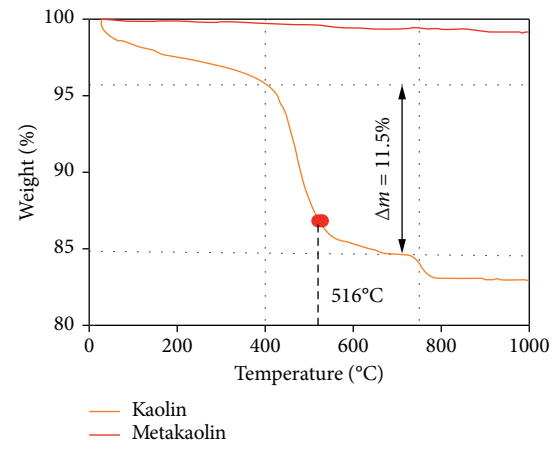

Figure 5: Thermogravimetric analysis curves of kaolin and metakaolin.

The results indicated that the weight of kaolin decreases by 11.2% at 400°C–750°C. The weight loss rate of metakaolin is less than 1.0%, indicating that dehydroxylation was completed during previous calcination. In addition, the weight loss of kaolin at 400°C–516°C is significantly greater than that at 516°C–750°C because the hydroxyl groups between the silicon tetrahedron and the aluminoxy octahedron cannot escape from the kaolin as rapidly as those present on the surface. Therefore, the hydroxyl groups require a slow migration process.

3.3. Infrared Spectroscopy (IR) Results. After calcination, the distribution of the hydroxyl groups in kaolin also changed. Figure 6 shows the IR spectra of metakaolin and kaolin.

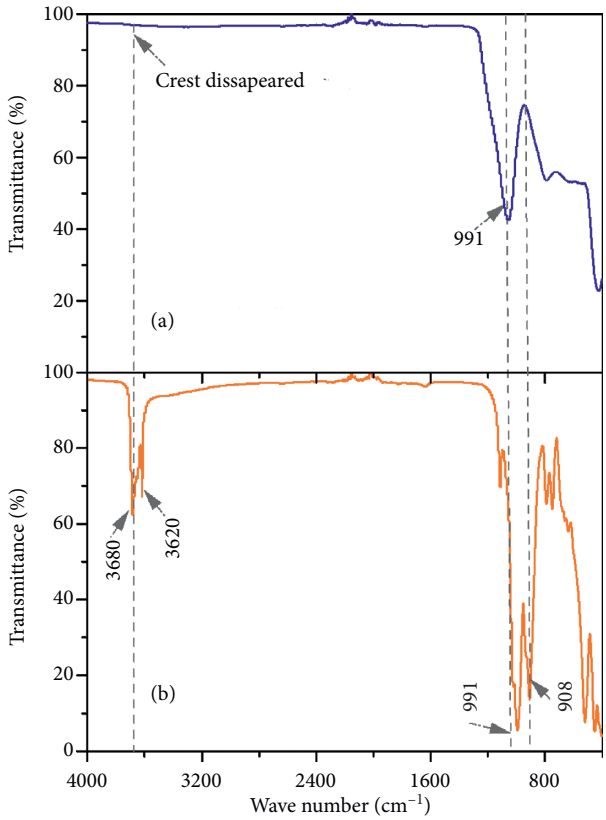

Figure 6: Infrared spectra of (a) metakaolin and (b) kaolin.

At a frequency range of 3200–4000 cm^{-1}, kaolin exhibited bands at 3680 and 3620 cm^{-1}, corresponding to the elongation vibrations of the hydroxyl group, and the band at 991 cm^{-1} corresponds to the Si-O-Si elongation vibrations. The band at 908 cm^{-1} corresponds to the deformation vibrations of the Al-O-H hydroxyl groups on the alumina faces [17] (Figure 6). After calcination, kaolin was transforms into metakaolin. Four major changes are observed in the IR spectrum (Figure 6(a)). (1) The peak corresponding to the hydroxyl-bonded water disappear; (2) the peak corresponding to Si-O-Si become broad and short; (3) the peak corresponding to Al-O-H nearly disappear; (4) the peak corresponding to Si-O-Al or Si-O-Mg observed at less than 800 cm^{-1} almost disappear. As described above, the combined water and structural water evaporated, and the spatial arrangement of Si-O-Si, Si-O-Al, or Si-O-Mg in kaolin change during calcination. In addition, notably, the high reactivity of metakaolin has been reported to be also related to a change in the Al^{3+} coordination from octahedral in kaolin to tetrahedral in metakaolin (tetrahedral Al^{3+} is typically more reactive than octahedral Al^{3+} [22]. Therefore, the high-temperature treatment leads to the increased activities of the silicon- and aluminium-containing groups, and these groups readily react with the calcium ions in the alkaline solution. In fact, a small amount of aggregate may be formed in metakaolin due to electrostatic interactions between the edge and surface of the basic unit structure or incomplete dehydroxylation, during which the structure is transforms from the original face-to-face "stacked" structure to an edge-to-surface "overlapped" shape (it can be seen clearly in SEM results (Figure 7)).

Clearly, metakaolin calcined from kaolin comprises silica and alumina, and kaolinite is the main mineral in laterite. The potential method for stabilizing laterite with metakaolin and lime was found to be efficient and environmentally friendly.

3.4. Shrinkage Strength and Microtest Results. Figure 8 shows the shrinkage curves of the compacted specimens (La, LaL, and LaLM). All samples exhibit a shrinkage limit of 25%, and the linear shrinkage of LaL decreases from 1.95% to 0.91%. Notably, the linear shrinkage of LaLM decreases by nearly a factor of 8 to 0.25%, indicating that metakaolin can help lime to considerably hinder the shrinkage of laterite.

Figure 9 shows the change in the suction of the compacted specimens (La, LaL, and LaLM) with the water content.

Two series of samples were investigated: saturated and unsaturated. With the decrease in the water content, suction gradually increase, especially at a water content of less than 7.5%. With the increase in suction, the strength of the unsaturated soils increases. However, at a water content of less than 25%, the UCS of compacted laterite remained 2.0 MPa. Notably, at an extremely low water content, the UCS decrease. The saturated compacted laterite exhibits a similar variation, but its UCS is typically less than that of compacted laterite without dehydration at a water content of less than 25% (Figure 10(a)). Kong et al. [23] have proposed that microcracks are formed in samples during dehydration, and the contribution of suction to the strength was opposed by the structural damage from the microcracks, which explains the phenomenon in Figure 10(a) (left). Nie et al. [24] has hypothesises that saturation destroys the existing structures or particle bonding in samples; this process can decrease the strength of compacted laterite, which would explain the curve in Figure 10(a) (right).

Although the strengths of LaL and LaLM decrease during dehydration, the values still exceed 2.0 MPa under different moisture conditions in contrast to that of laterite. In contrast, the strengths of LaL and LaLM increase rather than consistently decrease, which is similar to that observed for completely dried laterite samples (Figure 10(b)). This result indicates that lime or metakaolin and lime can improve the strength of laterite during dehydration. To further investigate the effect of dehydration on the compacted samples, direct shear strength was determined at the same time. Figure 11 shows the relationship between the direct shear strength and water content.

The direct shear strengths of LaL and LaLM are always greater than that of compacted laterite, and the strength of compacted laterite initially increases and reaches a peak of 0.5 MPa at a water content of 25%, which is near the shrinkage limit (Figure 8); this peak is followed by a decreasing trend until a water content of 15% is attained. The shear strength of compacted laterite reaches the peak at a water content of 27.5% during dehydration. For treated soil, the shear strength reaches the peak at a water content

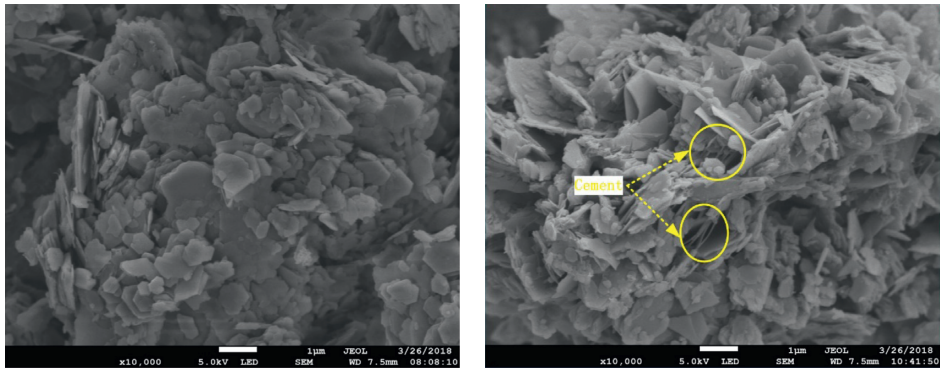

(a) (b)

Figure 7: SEM images of (a) lime-kaolinite and (b) lime-metakaolin.

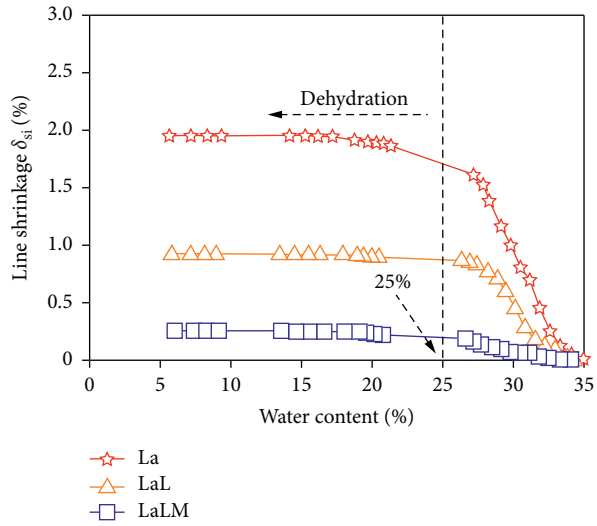

Figure 8: Shrinkage curves of treated and untreated laterite.

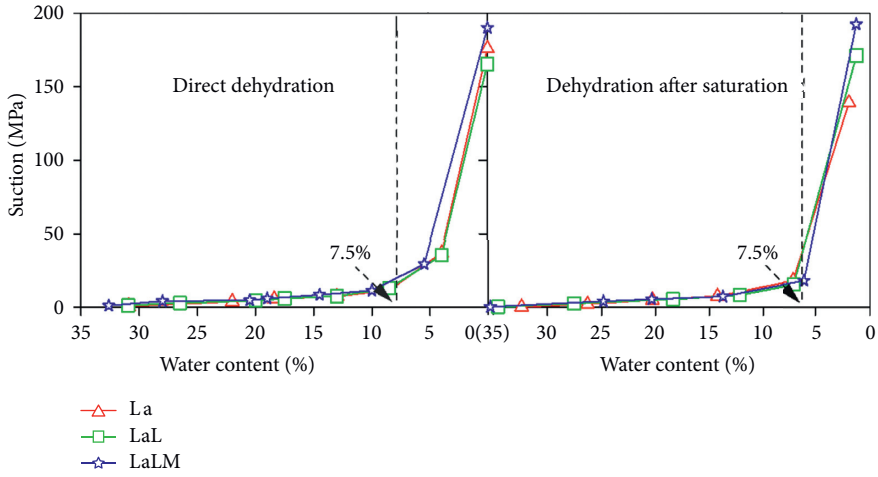

Figure 9: Suction as a function of water content.

of 25%, followed by a decreasing trend. In addition, similar trends are observed in the UCS tests. The UCS of untreated soil exhibits lower strength at all water contents after the samples reach saturation, and the treated soil maintains its strength even after saturation. Yang [25] has reported that several reticular cement substances are formed after the

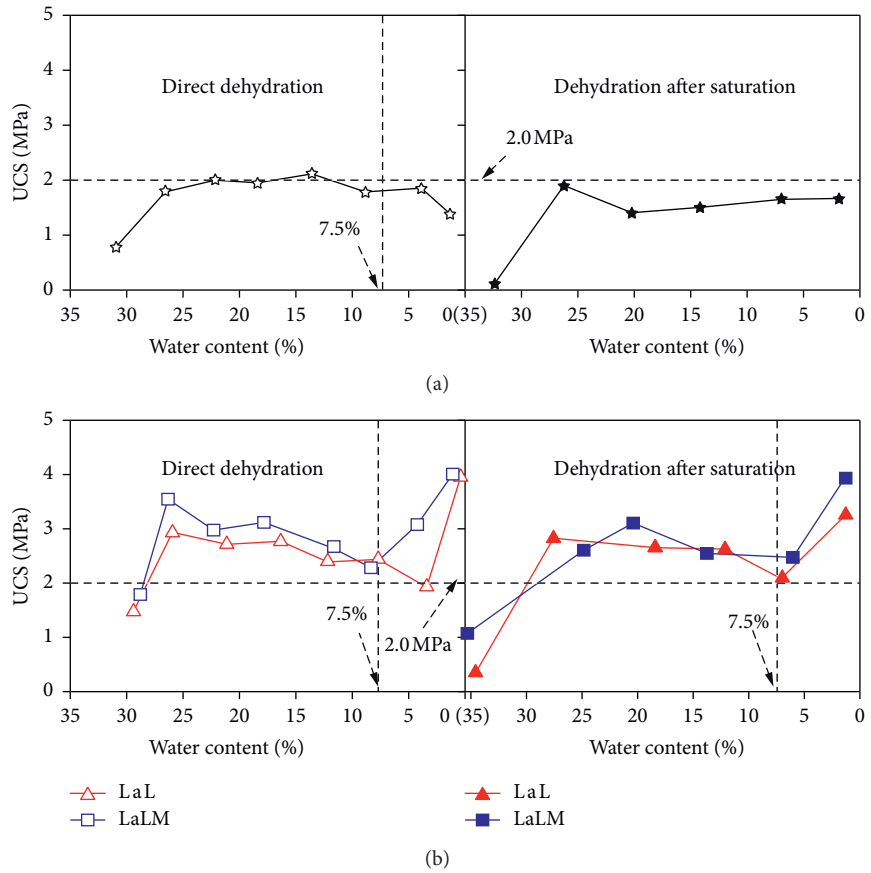

Figure 10: UCS as a function of water content. (a) Laterite. (b) Treated laterite.

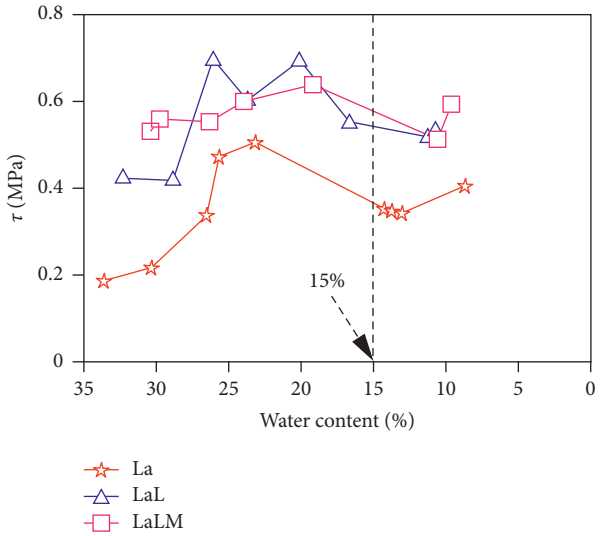

Figure 11: Peaks of direct shear strength vs. moisture content.

addition of lime to laterite; these cements connect the soil particles into a whole to resist the strength decrease during dehydration. Surprisingly, the direct shear strength of compacted laterite tends to increase at a water content of less than 15%, which is related to the friction between laterite aggregates due to dehydration under a vertical stress of 200 kPa.

The ability of metakaolin to enhance the inhibitory effect of lime on the shrinkage of laterite can be attributed to its composition and structure. Figure 7 shows the SEM micrographs of the structures of kaolin and metakaolin by the addition of lime after curing for 28 days. Metakaolin is characterised by an important structural disorder, such as the deformation of the silica network, permitting the facile capture of calcium ions in the hydrated lime solution due to its high pozzolanic activity. A larger amount of cementite was formed from the mixture of lime-metakaolin than that from the mixture of lime-kaolin under the same curing conditions.

Metakaolin exhibits a substantial ability to catch calcium ions, changing the calcium-ion concentration in the treated soil (Figure 12). The content of calcium ions in LaLM is less than that in LaL (Figure 12). This result can be extrapolated to reveal that metakaolin efficiently adsorbs calcium ions. Therefore, metakaolin and lime can rapidly generate a large amount of cement between laterite clusters (particles) more than lime-laterite, increase the overall adhesion of laterite particles, and improve the strength of laterite.

The molecular structure of metakaolin plays an important role in its ability to efficiently adsorb calcium ions from solutions. Konan et al. [17] have reported that kaolin adsorbs calcium hydroxide not only at the edges of the clay particles but also on the basal faces (Figure 4). As kaolin comprises a laminated structure, the adsorbed hydrated

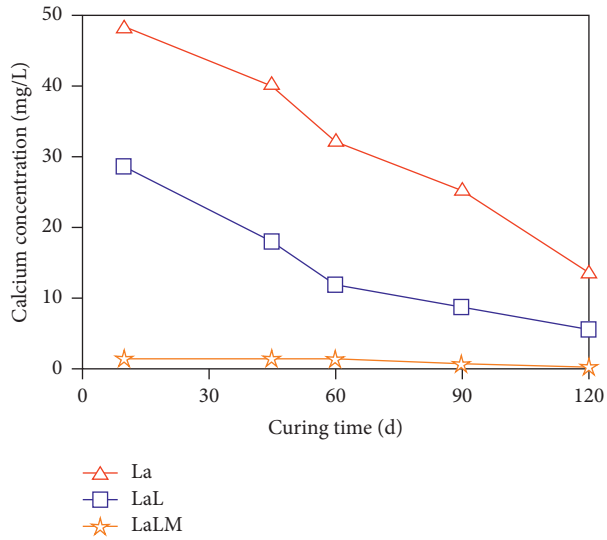

Figure 12: Calcium concentration as a function of curing time.

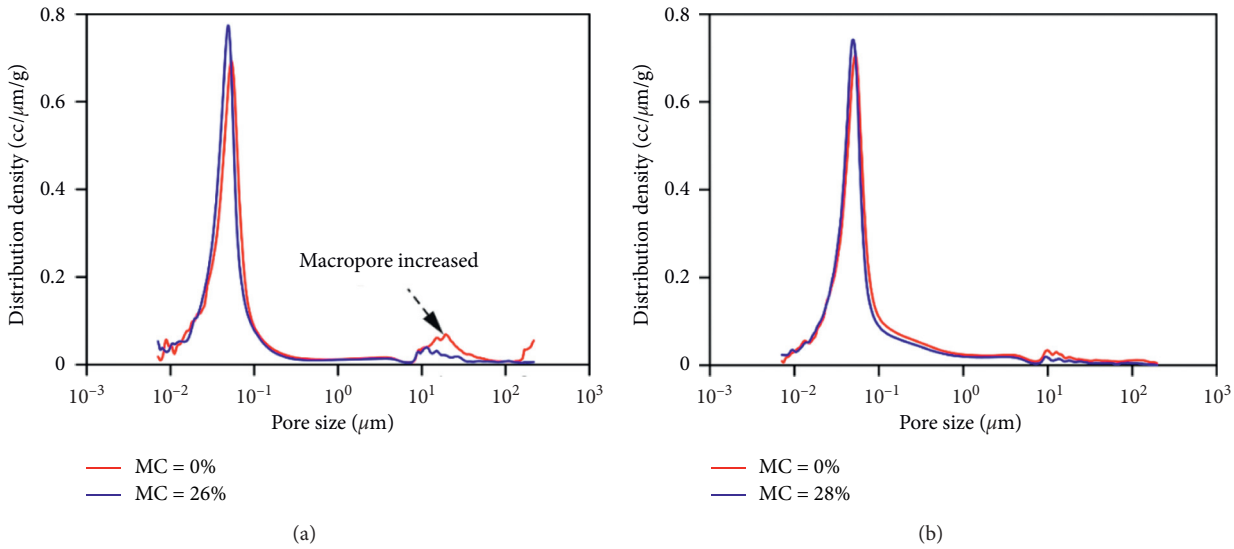

Figure 13: Pore size distributions of treated laterite. (a) LaL. (b) LaLM.

calcium ions form a layer on the clay particle surfaces, preventing the further dissolution of the clay mineral platelets [26]. Metakaolin comprises several amorphous silicon and aluminium oxides, enabling the rapid formation of hydrated phases at the interfaces between metakaolin and lime solutions and rendering high structural strength between the laterite aggregates. The results can be attributed to the special "overlapping" edge-surface structure.

The comparison of the pore distributions of the two samples (LaL and LaLM, respectively) clearly reveals that if only lime is added to laterite, pores between 10 μm and 100 μm (Figure 13(a)) increase during dehydration. However, with the addition of both lime and metakaolin to laterite, the pores barely change (Figure 13(b)), also indicating that metakaolin can enhance the structure of lime-stabilized soil, hinder shrinkage, and prevent microfissure development.

4. Conclusions

In this study, a series of tests were conducted on three samples (La, LaL, and LaLM, respectively) to determine the shrinkage, UCS, suction, direct shear strength, and pore size distribution. In addition, the shrinkage mechanism of laterite modified by lime and metakaolin was examined. The following conclusions can be drawn:

(1) After calcination, not only the hydroxyl groups disappeared but also the spatial structures of Si-O-Si and Si-O-Al (Mg) in kaolin are changed.

(2) Although the suction of compacted laterite increases during dehydration, microcracks are observed during this period, thereby impairing the strength of laterite. In addition, metakaolin is found to enhance the decrease shrinkage of laterite and increase the strength overall.

(3) The microscopic examination of metakaolin reveals a substantial amount of amorphous silicon and aluminium oxides and shares edge-surface contact structures, thereby enabling it to significantly capture calcium ions in the lime solution and subsequently generating cementitious hydrates in the interaggregates of laterite.

Data Availability

The authors declare that all the data presented in the manuscript were obtained from laboratory tests at China Three Gorges University in Yichang Hubei China. All the laboratory testing data were presented in the figures and tables in the manuscript. The data used in the study are available from the corresponding author upon request.

Conflicts of Interest

The authors declare no conflicts of interest.

Acknowledgments

This study was financially supported by the National Natural Science Foundation of China (51579137 and 51979150) and Youth Innovation Team Project of Hubei Province (T201803).

References

[1] M. D. Gidigasu, *Laterite Soil Engineering: Pedogenesis and Engineering Principles*, Elsevier Scientific Publishing Company, New York, NY, USA, 1976.

[2] Y. H. Wang, "Definition and demonstration of laterite," in *Proceedings of the Second National Symposium on Laterite Engineering and Geology*, Guizhou Science And Technology Press, Guizhou, China, pp. 11–20, 1991.

[3] H. S. Yang, H. Wei, Y. L. Yang, J. Y. Li, and X. L. Yin, "Deterioration reaction between alkali materials and laterite dam," *Chinese Journal of Geotechnical Engineering*, vol. 34, no. 1, pp. 189–192, 2012.

[4] K. Mu, L. W. Kong, X. W. Zhang, and S. Yin, "Experimental investigation on engineering behaviors of red clay under effect of wetting-drying cycles," *Rock and Soil Mechanics*, vol. 37, no. 8, pp. 2247–2253, 2016.

[5] D. L. Wang, M. T. Luan, and Q. Yang, "Experimental study on unsaturated remoulded clay subjected to drying and wetting cycle paths," *Chinese Journal of Rock Mechanics and Engineering*, vol. 26, no. 9, pp. 1862–1867, 2007.

[6] X. W. Liu, L. J. Chang, and X. R. Hu, "Experimental research of matric suction with water content and dry density of unsaturated laterite," *Rock and Soil Mechanics*, vol. 30, no. 11, pp. 3302–3306, 2009.

[7] C. N. Shen, X. W. Fang, H. W. Wang, S. G. Sun, and J. F. Guo, "Research on effects of suction, water content and dry density on shear strength of remoulded unsaturated soils," *Rock and Soil Mechanics*, vol. 30, no. 5, pp. 1347–1351, 2009.

[8] P. H. Morris, J. Graham, and D. J. Williams, "Cracking in drying soils," *Canadian Geotechnical Journal*, vol. 29, no. 2, pp. 263–277, 1992.

[9] C. S. Tang, B. Shi, C. Liu, L. P. Zhao, and B. J. Wang, "Influencing factors of geometrical structure of surface shrinkage cracks in clayey soils," *Engineering Geology*, vol. 101, no. 3-4, pp. 204–217, 2008.

[10] Y. Z. Tan, B. Yu, X. L. Liu, Z. Wan, and H. X. Wang, "Pore size evolution of compacted laterite under desiccation shrinkage process effects," *Rock and Soil Mechanics*, vol. 36, no. 2, pp. 369–375, 2015.

[11] S. L. Wen, J. L. Ren, Z. Q. Jiang, and Z. Q. Li, "Case analysis of red clay gravel pile composite foundation," *Chinese Journal of Geotechnical Engineering*, vol. 32, no. 2, pp. 302–305, 2010.

[12] J. Peng, J. Zhang, J. Li, Y. Yao, and A. Zhang, "Modeling humidity and stress-dependent subgrade soils in flexible pavements," *Computers and Geotechnics*, vol. 120, p. 103413, 2020.

[13] J. Zhang, L. Ding, F. Li, and J. Peng, "Recycled aggregates from construction and demolition wastes as alternative filling materials for highway subgrades in China," *Journal of Cleaner Production*, vol. 255, Article ID 120223, 2020.

[14] F. G. Bell, "Lime stabilization of clay minerals and soils," *Engineering Geology*, vol. 42, no. 6, pp. 223–237, 1996.

[15] C.-S. Poon, L. Lam, S. C. Kou, Y.-L. Wong, and R. Wong, "Rate of pozzolanic reaction of metakaolin in high-performance cement pastes," *Cement and Concrete Research*, vol. 31, no. 9, pp. 1301–1306, 2001.

[16] A. Shvarzman, K. Kovler, G. S. Grader, and G. E. Shter, "The effect of dehydroxylation/amorphization degree on pozzolanic activity of kaolinite," *Cement and Concrete Research*, vol. 33, no. 3, pp. 405–416, 2003.

[17] K. L. Konan, C. Peyratout, A. Smith, J.-P. Bonnet, S. Rossignol, and S. Oyetola, "Comparison of surface properties between kaolin and metakaolin in concentrated lime solutions," *Journal of Colloid and Interface Science*, vol. 339, no. 1, pp. 103–109, 2009.

[18] J. J. Brooks and M. A. Megat Johari, "Effect of metakaolin on creep and shrinkage of concrete," *Cement and Concrete Composites*, vol. 23, no. 6, pp. 495–502, 2001.

[19] Ministry of Transport of the People's Republic of China, *JTG E40-2007 Test Methods of Soils for Highway Engineering*, Ministry of Transport of the People's Republic of China, Beijing, China, 2007, in Chinese.

[20] G. Kakali, T. Perraki, S. Tsivilis, and E. Badogiannis, "Thermal treatment of kaolin: the effect of mineralogy on the pozzolanic activity," *Applied Clay Science*, vol. 20, no. 1-2, pp. 73–80, 2001.

[21] H. H. Murray, "Applied clay mineralogy today and tomorrow," *Clay Minerals*, vol. 34, no. 1, pp. 39–49, 1999.

[22] C. Panagiotopoulou, E. Kontori, T. Perraki, and G. Kakali, "Dissolution of aluminosilicate minerals and by-products in alkaline media," *Journal of Materials Science*, vol. 42, no. 9, pp. 2967–2973, 2007.

[23] L. W. Kong, Y. W. Zhao, A. G. Guo, and Y. F. Tuo, "Analysis of engineering characters and mechanism of the dehumidification process of undisturbed laterite," in *Proceedings of the 9th Academic Conference of Soil Mechanics and Geotechnical Engineering, China Civil Engineering Society*, Tsinghua University Press, Beijing, China, pp. 424–427, 2003.

[24] Q. K. Nie, Y. H. Wang, S. Q. Liang, and Q. X. Zhang, "Water-sensitivity of compacted laterite clays in jingxi of Guangxi region," *Rock and Soil Mechanics*, vol. 31, no. 4, pp. 1134–1138, 2010.

[25] Z. Q. Yang and J. Y. Guo, "The physio-mechanical properties and micro-mechanism in lime-soil system," *Rock and Soil Mechanics*, vol. 12, no. 3, pp. 11–23, 1991.

[26] K. L. Konan, C. Peyratout, J.-P. Bonnet et al., "Surface properties of kaolin and illite suspensions in concentrated calcium hydroxide medium," *Journal of Colloid and Interface Science*, vol. 307, no. 1, pp. 101–108, 2007.